small NANO MICRO

DOI: 10.1002/smll.200800390

Charge Transport Through a Cardan-Joint Molecule

Mario Ruben, Aitor Landa, Emanuel Lörtscher,* Heike Riel, Marcel Mayor, Helmar Görls, Heiko B. Weber, Andreas Arnold, and Ferdinand Evers**

The charge transport through a single ruthenium atom clamped by two terpyridine hinges is investigated, both experimentally and theoretically. The metal-bis(terpyridyl) core is equipped with rigid, conjugated linkers of para-acetyl-mercapto phenylacetylene to establish electrical contact in a two-terminal configuration using Au electrodes. The structure of the $[Ru^{II}(\mathbf{L})_2](PF_6)_2$ molecule is determined using single-crystal X-ray crystallography, which yields good agreement with calculations based on density functional theory (DFT). By means of the mechanically controllable break-junction technique, current–voltage (I–V), characteristics of $[Ru^{II}(\mathbf{L})_2](PF_6)_2$ are acquired on a single-molecule level under ultra-high vacuum (UHV) conditions at various temperatures. These results are compared to ab initio transport calculations based on DFT. The simulations show that the cardan-joint structural element of the molecule controls the magnitude of the current. Moreover, the fluctuations in the cardan angle leave the positions of steps in the I–V curve largely invariant. As a consequence, the experimental I–V characteristics exhibit lowest-unoccupied-molecular-orbit-based conductance peaks at particular voltages, which are also found to be temperature independent.

Keywords:
- break junctions
- molecular electronics
- ruthenium complexes
- single-molecule studies

1. Introduction

A detailed understanding of charge transport through single-molecule junctions is a key prerequisite for the design and development of molecular electronic devices.[1] Various experimental techniques have been used to demonstrate transport through single molecules, for example, mechanically controllable break junctions (MCBJs),[2] electro-migrated junctions (EMJs),[3] and scanning tunneling microscopy/spectroscopy measurements (STM/STS).[4] Among the molecules of interest, the class of metal-ion complexes attracts special attention because the electron and spin densities of these complexes are highly confined, both electronically and spatially, around the metal centers, which means that they have a large potential for use in ''ion-dot'' concepts, analogous to larger quantum dots.[5] Pt^{II} and Fe^{II} compounds have been investigated in MCBJ experiments, and exhibited conductance values ranging from insulator like[6a] to metal like.[6b] Co^{II} and Os^{II} complexes bearing insulating linkers of different chain lengths have been studied in electro-migrated nano-gaps[7] and in in-situ STM/STS experiments, which revealed transistor-like behavior.[8]

[*] Dr. M. Ruben, Dr. F. Evers, Dr. A. Landa, Dr. A. Arnold
Institute of Nanotechnology, Karlsruhe Institute of Technology
PF 3640, 76021 Karlsruhe (Germany)
E-mail: ruben@int.fzk.de, evers@int.fzk.de
Dr. E. Lörtscher, Dr. H. Riel
IBM Zurich Research Laboratory
Säumerstrasse 4, 8803 Rüschlikon (Switzerland)
E-mail: hei@zurich.ibm.com
Dr. F. Evers
Institut für Theorie der Kondensierten Materie
Karlsruhe Institute of Technology
PF 6980, 76128 Karlsruhe (Germany)
Prof. M. Mayor
Department of Chemistry, Universität Basel
St. Johanns-Ring 19, 4056 Basel (Switzerland)
Dr. H. Görls
Institut für Anorganische und Analytische Chemie, Universität Jena
Agust-Bebel-Strasse 1, 07743 Jena (Germany)
Prof. H. B. Weber
Institut für Angewandte Physik, Universität Erlangen-Nürnberg Staudtstrasse 7, 91058 Erlangen (Germany)

Supporting Information is available on the WWW under http://www.small-journal.org or from the authors.

Herein, we report on single-molecule transport through a $[Ru^{II}(\mathbf{L})_2](PF_6)_2$ molecule (with **L** being thioacetic acid S-(4-[2,2′;6′,2″]terpyridin-4′-ylethynyl-phenyl ester)) using a two-terminal MCBJ configuration. The properties of this class of molecular compounds are well established in bulk chemistry as they offer a broad variety of technologically relevant properties, namely, their photo-physical, redox, and charge-transfer characteristics.[9] In particular, Ru(II) polypyridyl complexes act as photo sensitizers, making them interesting candidates for light-driven conversion processes such as artificial photosynthesis,[10] photocatalytic production of hydrogen,[11] dye-sensitized solar cells,[12] photon-induced switches,[13] and molecular machines.[14] The concept of a single metal atom held by polypyridyl ligands allows electrical contact to be established with a single atom in a very controlled way. As single metal atoms have several interesting characteristics (e.g., redox, magnetic, spin state, electronic transition, etc.), our work contributes to establishing a chemical, experimental, and theoretical base for future molecule-based electronics and spintronics.

2. Results and Discussion

2.1. Synthesis and Structure of $[Ru^{II}(L)_2](PF_6)_2$

The acetyl-protected dithiol compound $[Ru^{II}(\mathbf{L})_2](PF_6)_2$ was synthesized following a multistep reaction scheme involving several Pd-catalyzed Sonogashira couplings (see Supporting Information). Its structure was verified by single-crystal X-ray crystallography (Figure 1A and B). Compound $[Ru^{II}(\mathbf{L})_2](PF_6)_2$ crystallized in the triclinic space group *P*1, and the central Ru^{II} ion was coordinated in a slightly compressed octahedron by six N-donor atoms, putting the two neutral ligands **L** perpendicularly around the metal ion. As a consequence, the two elongated ligands pointed along the long axis of the molecule (with a slight distortion due to crystal-packing effects; N–Ru–N angle: 178.8°) forming two π-systems separated by the Ru^{II} metal ion. Thus, the Ru^{II} metal ion was held as single connection point between the two conjugated systems, and any conduction path was expected to pass through this atom.

The terpyridyl ligands were equipped with acetyl-protected alkenyl-thiophenyl linkers for anchoring the $[Ru^{II}(\mathbf{L})_2](PF_6)_2$ molecule to Au electrodes. The intramolecular sulfur–sulfur distance was determined from the X-ray structure to be 2.64 nm (Figure 1B and C). The core structure of the $[Ru^{II}(\mathbf{L})_2](PF_6)_2$ molecule closely resembled a mechanical Cardan joint, whereby the Ru^{II} metal ion acts as a junction between two orthogonally twisted ligand hinges. The connecting diamagnetic Ru^{II} metal ion interrupts the π-conjugation of the $[Ru^{II}(\mathbf{L})_2](PF_6)_2$ molecule, creating two fully conjugated organic subsystems that are twisted by 90°. The double-positively charged $[Ru^{II}(\mathbf{L})_2]^{2+}$ core is electrostatically compensated by two loosely-bound PF_6^- anions.

2.2. Single-Molecule Transport Measurements of $[Ru^{II}(L)_2](PF_6)_2$

The properties of charge transport through single molecules of the complex $[Ru^{II}(\mathbf{L})_2](PF_6)_2$ were investigated using

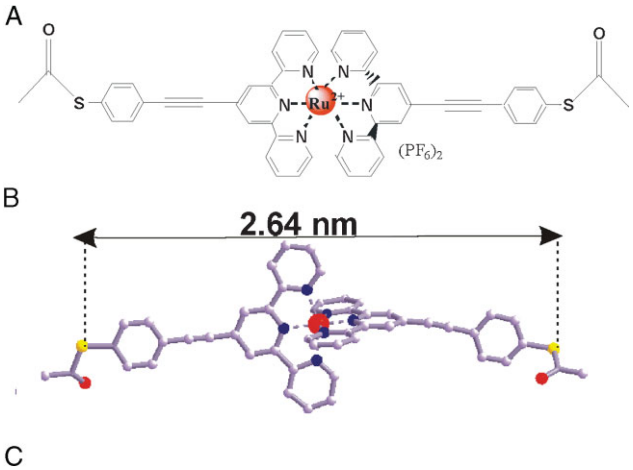

	X-ray	*DFT*
$Ru\text{-}N_{lateral}$	1.964	1.994
$Ru\text{-}N_{central}$	2.065	2.089
S-S	26.39	26.73

Figure 1. Molecular structure of complex $[Ru^{II}(\mathbf{L})_2](PF_6)_2$. A) Schematic representation of the molecule, and B) its molecular structure determined in a single-crystal diffraction study, showing the Cardan-type $[Ru(tpy)_2]$-core structure (Ru^{II}: red, N: blue; C: grey), the phenyl-acetylene linkers, and the acetyl-protected thiols groups (S: yellow, O: red; hydrogen atoms and PF_6^- anions have been omitted for clarity). C) Comparison of the averaged Ru^{II}–N bond lengths and of the lateral sulfur-to-sulfur (S–S) distance of $[Ru^{II}(\mathbf{L})_2](PF_6)_2$ determined by X-ray crystallography and DFT calculations for an isolated molecule (in Å). The small deviations between the experimental and the theoretical values are mainly ascribed to packing effects in crystallography.

the MCBJ[15] technique. Our MCBJ system operates under ultra-high vacuum (UHV) conditions (base pressure 4×10^{-9} mbar) at temperatures ranging from room temperature ($T = 300$ K) down to 4.2 K. An electrode pair with atomic-sized tips can be created using the MCBJ method. These tips are located exactly opposite each other, and their separation can be precisely adjusted with subatomic accuracy. Moreover, electrodes produced using the MCBJ technique are very stable against external vibrations and thermal drifts. This stability is gained through a purely mechanical working principle, using a three-point bending mechanism with a very low translation ratio, *r*, between the pushing-rod translation, Δh, and the electrode separation, Δd (see Figure 2). The ratio *r* is given by

$$r = \frac{\Delta d}{\Delta h} = \frac{6ts}{L^2} \quad (1)$$

where *s* is the length of the metal bridge, *t* the thickness of the substrate, and *L* the distance between the supports (see Figure 2B).

The sample manufacturing process is described in the Supporting Information. Using our geometry, a value of 2×10^{-5} is achieved for *r*. Hence, the distance between the electrodes can theoretically be controlled with picometer

NANO MICRO small

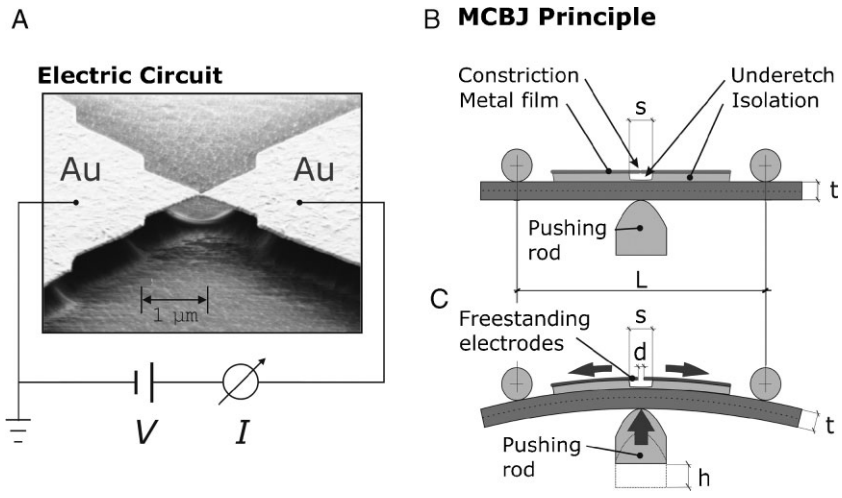

Figure 2. Principle of an MCBJ. A) Scanning electron microscopy image of microfabricated MCBJ sample consisting of freestanding metal bridge with a central lateral constriction on top of a flexible insulating substrate. The electrical circuit is schematically drawn. B) The MCBJ sample is mounted in a three-point bending mechanism. C) The bending force applied to the bottom of the substrate introduces surface extension, which elongates and finally breaks the metal bridge at its smallest constriction, creating two separated electrodes. The distance between the electrodes can be controlled in both the opening and the closing direction with subpicometer accuracy by bending or relaxing the sample.

accuracy. Microscopic changes of the tips during breaking prevent an absolute-distance calibration. Instead, a relative-distance calibration can be performed by analyzing the dependence of the tunneling current. Thereby the sample-specific ratio r is obtained.

Using this calibration, d is set to be longer than the length of the molecule under investigation prior to molecule deposition. The compound $[Ru^{II}(\mathbf{L})_2](PF_6)_2$ is terminated by acetyl-protected sulfur anchor groups, which are suited to bridging the gap between the two electrodes (see Figure 1A). The compound is dissolved in a methanol/tetrahydrofuran (1:9) mixture in a concentration of 5×10^{-4} mol L^{-1}. The molecules are applied on the gold electrodes by depositing a droplet of this solution onto the open junction. As illustrated in our earlier experiments,[16–18] the acetyl protection group hydrolyzes on the gold surface upon contact with Au, and the molecule establishes a covalent bond to one of the two Au electrodes via a thiol anchor group. After solvent evaporation, the chamber is evacuated, and measurements are started when UHV conditions have been reached (5×10^{-8} mbar).

When slowly closing the electrodes under a fixed bias (2–20 mV), the formation of a molecular junction is indicated by an intermediate resistance (R) regime between the fully open ($R > 1$ TΩ) and the fully closed ($R \leq 12.9$ kΩ) junction. The appearance of such an intermediate regime in the closing and the opening of the junction strongly differs from the tunneling characteristic, which is measured in the absence of molecules. This intermediate regime can therefore be attributed to the formation of a molecular junction. Instead of applying a small constant voltage to determine the conductance of a molecule, we are interested in studying the transport properties over a broad voltage range, in which the first molecular orbital in resonance (typically 0.5–2.5 V) can be probed. Therefore, we concurrently acquire current–voltage (I–V) curves during the stepwise closing and opening of the junction. Thus, we can measure the transport properties of the molecular junction during formation and breaking.[18] After junction formation, the Au–molecule–Au system was cooled down. At low temperatures, electrode stability is improved significantly compared with room temperature because of the reduced surface mobility of the gold atoms.

Figure 3 shows I–V and differential conductance (G_{Diff}–V) data recorded at three different temperatures using three different samples and the measurement protocol described elsewhere.[18] To obtain G_{Diff}, the current data acquired were averaged over three data points prior to numerical derivation. The I–V measurements of the Au–$[Ru^{II}(\mathbf{L})_2](PF_6)_2$–Au system were performed below room temperature to guarantee reproducible data acquisition. At 250 K, two peaks in the G_{Diff}–V data were revealed (Figure 3A), defining a conductance gap of approximately 0.8 eV. At this voltage, the first molecular orbital aligns with the chemical potential of one electrode, and resonant transport across this particular molecular orbital occurs. At 50 K, the conductance gap is maintained and the signal-to-noise ratio is significantly improved compared with 250 K (Figure 3B).

At 10 K, further conductance peaks appear at lower and higher voltages of approximately −0.6 V and +1.1 V, as indicated in Figure 3C. Moreover, the first peaks defining the conductance gap are found to be less pronounced than at 50 or 250 K. However, in the logarithmic representation (inset in Figure 3C) the distinct difference between the gap regime, in which off-resonance transport based on tunneling between the electrodes occurs, and the resonant regime, in which resonant transport through molecular orbitals takes place, becomes evident. Overall, the absolute current amplitude decreases with decreasing temperature at a given voltage.

The design of the Cardan-joint-type structure of the $[Ru^{II}(\mathbf{L})_2]^{2+}$ core creates a situation in which all current flowing through the Au–$[Ru^{II}(\mathbf{L})_2](PF_6)_2$–Au system has to pass through the Ru^{II} metal ion, as this ion is the single connection point of the two ligand hinges. We have found indications of the flexibility of the Cardan joint in the behavior of the Au–$[Ru^{II}(\mathbf{L})_2](PF_6)_2$–Au molecular junction upon manipulation. First, stable and reproducible I–V curves are only acquired in the opening cycle of our approach.[18] Here, the Au–$[Ru^{II}(\mathbf{L})_2](PF_6)_2$–Au system is stretched, whereupon the transport properties measured are largely unaffected. This indicates that the Ru^{II}–terpyridine joint withstands the mechanical stretching force during opening of the molecular junction. Second, when opening and closing at a constant voltage (e.g., 5 mV), the intermediate regime in which the molecule is contacted (see Ref. [18] for more information) is substantially longer for the Au–$[Ru^{II}(\mathbf{L})_2](PF_6)_2$–Au system than for molecules with a comparable length of 2–3 nm. This

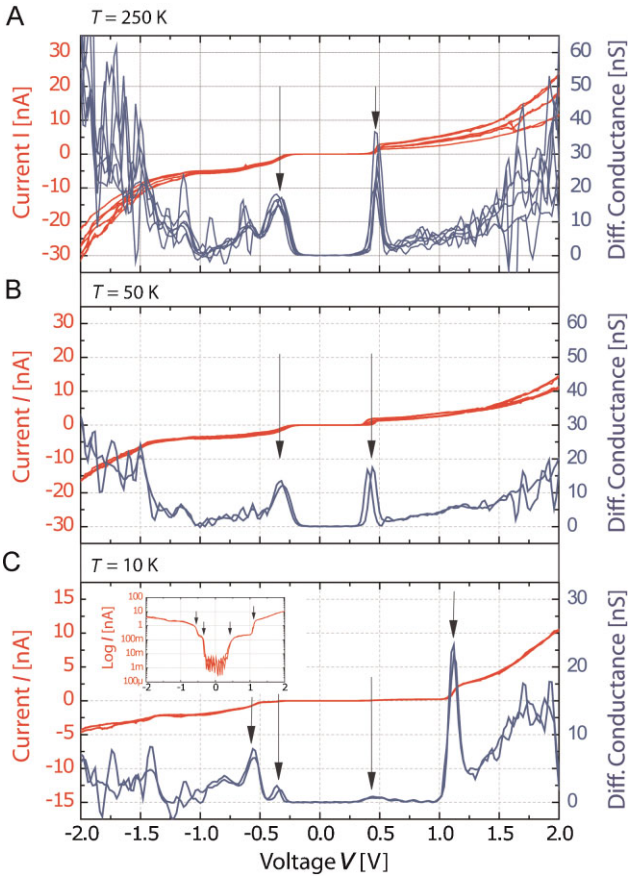

Figure 3. Electronic transport properties of Au-$[Ru^{II}(\mathbf{L})_2](PF_6)_2$-Au at different temperatures. A) At 250 K, a conductance gap of approximately 0.8 eV appears. B) At 50 K, the conductance gap is maintained and the signal-to-noise ratio is significantly improved. C) At lower temperatures (10 K), a second conductance peak appears, and the first peak is less pronounced. The log-scale inset clearly shows the presence of the conductance gap.

indicates that the Cardan joint enables the $[Ru^{II}(\mathbf{L})_2](PF_6)_2$ molecule to adjust to the altered gap distance without losing contact with the Au electrodes.

2.3. Ab Inito Transport Calculation of $[Ru^{II}(L)_2](PF_6)_2$

Ab initio transport calculations for $[Ru^{II}(\mathbf{L})_2](PF_6)$ are not standard because of the large size of the molecule and because part of the electrodes need to be included for a proper description of the hybridization of molecular orbitals with the surface states of the leads. To achieve the system sizes needed, we employed ground-state density functional theory (DFT, see Computational in Experimental Section). It was found that at low voltages the low-lying unoccupied molecular orbitals carry most of the current. This finding can be rationalized in the following manner. It is well known that an octahedral ligand field produces a large energy gap ($\Delta_{oct} \approx 3$ eV according to our calculations) in isolated Ru^{II} metal ions between occupied d states with t_{2g} and states with e_g character.[19a,20] After coupling the Ru^{II} atom to the terpyridyl cage (forming an approximately octahedral ligand field), hybrid states involving t_{2g} Ru valence orbitals and ligand states form with energy below or near E_F. Almost all of them are occupied to give the Ru^{II} its proper charge. Only very few t_{2g} hybrid states exhibit an energy above E_F and therefore remain empty. These states are situated mainly on the ligand system. They form the low-lying unoccupied states, in particular the lowest unoccupied molecular orbit (LUMO). The situation is reminiscent of studies of the metal-to-ligand charge transfer (MLCT) processes during low-energy electronic excitations.[21] By contrast, the (geometry-discouraged) e_g-type states have an energy well above the hybrid band. They do not participate in transport phenomena at low biases. Whether one observes electron (LUMO) or hole (HOMO) transport at low V_{bias} values depends on whether E_F is situated closer to the occupied t_{2g} hybrids or to the unoccupied LUMO states. Indeed, according to our calculations, the low-lying unoccupied t_{2g}-type hybrid orbitals have an energy ≈ 0.1 eV above E_F, whereas for the corresponding occupied orbitals we find an energy of ≈ -0.7 eV so that electron transport is predicted.

The LUMO is shown in Figure 4. The one-sided nature of the orbital indicates that, indeed, the connection between left and right is mediated by the Ru^{II} core only. Consequently, almost the entire current flows across the single metal atom. In this situation, the spin state of the center atom is of particular importance because a nonzero magnetization could invoke an Abrikosov–Suhl resonance at the Fermi energy, which in turn can be seen as a Kondo peak in the I–V curves. Our calculations indicate that the effect of the electrodes on the Ru atom is very small. As, after coupling to the electrodes, the (bare) energy gap Δ_{oct} between the Ru^{II}-t_{2g} and the Ru^{II}-e_g orbitals is large, the Ru^{II} state persists at $S = 0$, as in the free molecule. Hence, no correlation-induced increase of the zero-bias conductance is expected. The energy difference, Δ, between the LUMO and the Fermi energy of bulk gold, E_F, is related to a voltage difference $\approx V_c/2$, for which the bare DFT result is $\Delta \approx 0.1$ eV. One expects to observe a strong current increase in the I–V at bias voltages $V > V_c$, which indeed is seen in the theoretical I–V curve (Figure 5).

In addition to the transport gap, Figure 5 suggests that the second major peak in the differential conductance occurs only at $V_{bias} \geq 1$ V, where the (relatively broad) HOMO resonance enters the voltage window. Although there are clear qualitative theoretical predictions for the I–V curve, a reliable quantitative analysis is extremely difficult. In addition to the well-known methodological difficulties of DFT-based transport calculations, the Ru^{II} complex poses two more challenges for a

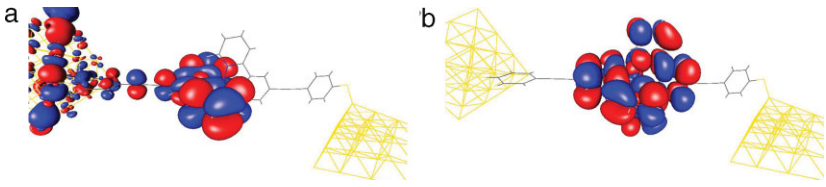

Figure 4. Wave-function intensity of the lowest unoccupied Kohn–Sham orbitals. A) LUMO, 0.06 eV above E_F; B) LUMO+1, 0.1 eV above E_F (The (right-sided) symmetry partner of LUMO is not shown). Red indicates regions with positive and blue with negative wavefunction amplitude. Also shown are the Au_{30} electrodes used in the calculation.

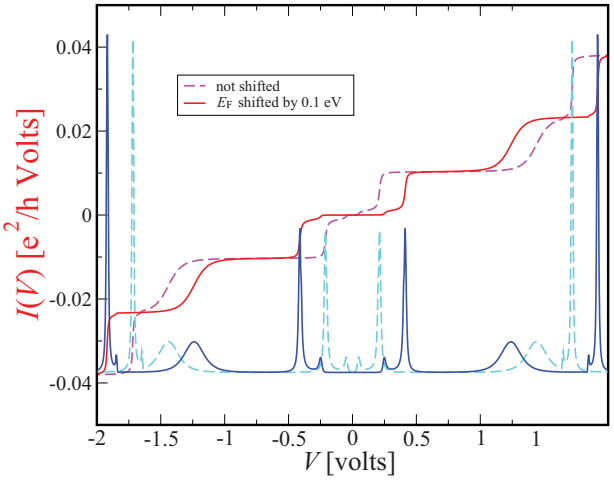

Figure 5. *I–V* curve for the Ru^{II} complex calculated by integrating the transmission function as obtained from Landauer–Büttiker theory. The dashed lines indicate the ab initio calculation without any fit parameter. To demonstrate the impact of the Fermi-level mismatch, the solid lines represent the *I–V* curves after shifting the Fermi energy up by 0.1 eV.

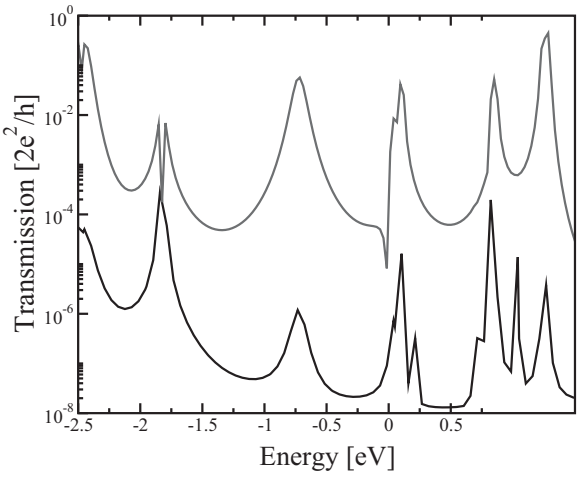

Figure 6. Transmission function for the straight molecule (Au_{30} calculation; black trace, perpendicular terpyridyl groups, zero bending) and with a Cardan angle of 10° (grey trace).

predictive analysis. i) The size of the complex is very large, so that the alignment of the Au Fermi level and the molecular levels is not described very accurately, although the simulation systems are already extremely large. As a consequence of this limitation (and others related to exchange correlation functionals), the estimate of Δ has an uncertainty of a few tenths of an eV. ii) The Ru^{II} atom connecting the two halves of the molecule is actually a very flexible (''cardanic'') joint, in which bending the molecule costs only 150 meV for every 10°. As this Cardan-joint aspect of the molecule is very interesting in itself, we now discuss it in more detail. The transmission is extremely sensitive to the bending angle, as can be inferred from Figure 6. For the straight molecule (zero bending angle), transmission is strongly suppressed. The perfect octahedral symmetry ensures that the t_{2g} orbitals direct the current through a narrow region close to the Ru^{II} core.

By contrast, bending re-mixes these states, and the wavefunction overlap increases again. Because only regions with small wavefunction amplitudes are involved, the transmission coefficients can change drastically, while the resonance energies are almost invariant. In a realistic experimental situation, the statistics of the molecular bending angle, and the bending angle itself, are not known. Therefore, a direct quantitative comparison between experimental and theoretical conductance values is not meaningful. However, resonance positions may be compared. A qualitative theoretical prediction for experimental observations is as follows: a broad spectrum of (differential) *I–V* curves may be found, reflecting the sensitivity of transport to the boundary conditions (e.g., stress, contact details) felt by the molecule. All traces should have one common feature, however, which is that current increases are situated at very similar energies.

Indeed, the threshold behavior of the current is seen in experiments at $V_c \approx 0.4$ V (the deviation from the bare theoretical value is easily explained, e.g., by a slight uncertainty of 0.1 eV in the Fermi energy, Figure 6). This threshold voltage persists at any temperature $T = 250$, 50, or 10 K, even though the peak values are quite different at the lowest T and the symmetry of the curve is completely lost. We propose the following to explain this last and striking feature: in a situation with nonzero bending angle, a strictly left–right symmetric arrangement of the molecule between the contacts (left and right) is highly improbable. For this reason, each half of the molecule will, in general, experience a slightly different bias voltage drop. Hence, the feedback of this potential drop differs for right- and left-sided molecular orbitals. As transport is very sensitive to the details of the orbitals in the vicinity of the Ru^{II} core, pronounced asymmetries could appear in the *I–V* curve at unusually small voltages. Such asymmetries are not necessarily apparent in the high-temperature data, Figure 3a, where the experimental data may be understood as an incoherent average over many microscopic junction configurations. At low temperatures, however, the junction is frozen, and here its unique polarization properties can reveal themselves more clearly, as observed in Figure 3c.

3. Conclusions

The electronic transport properties of a Cardan-joint-type molecule, $[Ru^{II}(\mathbf{L})_2](PF_6)_2$, have been investigated experimentally at different temperatures and compared with DFT calculations. Experimentally obtained *I–V* curves reveal reproducible characteristics with typical conductance peaks at a particular voltage of ±0.4 V. Ab initio calculations suggest that this value indicates resonant transport through the LUMO of the molecule. The reproducibility of peak positions is not obvious, given that a sizable experimental variability of the Cardan angle in $[Ru^{II}(\mathbf{L})_2](PF_6)_2$ is likely to be realized. Theory suggests that the observed reproducibility relates to the fact that the orbital energies are insensitive to the Cardan angle, in contrast to the orbital overlap, and hence the transmission occurs. Our study shows that the MCBJ technique is sufficiently versatile to perform controlled single-molecule transport

studies even with relatively large and flexible Cardan-joint molecules. The modular variability of the tested $[M^{II}(\mathbf{L})_2]^{2+}$ family with a broad accessibility to very different d-metal ions that exhibit interesting redox, magnetic, and spin-state properties sets the experimental base for further studies to promote molecule-based electronics and spintronics.

4. Experimental Section

Synthesis: All chemicals were of the highest available grade. The linker-modified terpyridine ligand **L** was synthesized as described in the supporting material. The complex $[Ru^{II}(\mathbf{L})_2](PF_6)_2$ was synthesized as follows: a solution of the terpyridine ligand **L** (100 mg, 0.23 mmol) and $Ru(DMSO)_4Cl_2$ (51.8 mg, 0.108 mmol) in ethanol/H_2O (50 mL/2.5 mL) was stirred at 70 °C for 3 h. The solvents were evaporated, and the crude was dissolved in the minimum amount of CH_3CN. Treatment of the solution with NH_4PF_6 (0.3 g in 5 mL H_2O) resulted in precipitation of a dark orange solid. The precipitate obtained was recrystallized twice in $CH_3CN/(l\text{-}Pro)_2O$ to yield analytically pure crystalline complex (53 mg, 41% yield). ^{1}H NMR (CD_3CN, δ): 8.92 (s, 4H), 8.53 (d, $J = 7.98$ Hz, 4H), 7.98 (dt, $J = 7.96$ Hz, $J' = 1.28$ Hz, 4H), 7.85 (d, $J = 8.49$ Hz, 4H), 7.64 (d, $J = 8.45$ Hz, 4H), 7.44 (d, $J = 4.82$ Hz, 4H), 7.21 (dd, $J = 7.16$ Hz, $J' = 1.19$ Hz, 4H), 2.49 (s, 6H); ^{13}C NMR (CD_3CN, δ): 194.1, 158.4, 156.2, 153.7, 139.3, 135.8, 133.6, 131.8, 130.9, 128.7, 126.3, 125.6, 123.3, 96.8, 88.4, 30.5 ppm; IR (KBr): $\nu = 3433$, 2218, 1705, 837 cm^{-1}; MALDI-TOF-MS: 917.3 [M^++H–2PF_6]. Crystals suitable for X-ray investigations were obtained from acetonitrile solution by diffusing di-isopropyl ether.

Crystal structure determination: The intensity data for the compounds were collected on a Nonius KappaCCD diffractometer, using graphite-monochromated Mo Kα radiation. Data were corrected for Lorentz and polarization effects, but not for absorption effects.[22,23] The structures were solved by direct methods (SHELXS)[24] and refined by full-matrix least-squares techniques against Fo^2 (SHELXL-97).[25] All hydrogen atoms were included at calculated positions with fixed thermal parameters. All nonhydrogen, nondisordered atoms were refined anisotropically.[25] XP (SIEMENS Analytical X-ray Instruments, Inc.) was used for structure representations.

Crystal data for **1**:[26] $C_{50}H_{34}F_{12}N_6O_2P_2RuS_2$, $Mr = 1205.96$ g mol^{-1}, red-brown prism, size $0.02 \times 0.02 \times 0.01$ mm^3, triclinic, space group P$\bar{1}$, $a = 9.3523(8)$, $b = 14.0731(14)$, $c = 19.799(2)$ Å, $\alpha = 100.422(5)$, $\beta = 103.032(6)$, $\gamma = 99.992(7)°$, $V = 2\,433.6(4)$ Å^3, $T = -90$ °C, $Z = 2$, $\rho_{calcd.} = 1.646$ g cm^{-3}, μ(Mo Kα) = 5.69 cm^{-1}, $F(000) = 1\,212$, 14 712 reflections in $h(-11/12)$, $k(-17/17)$, $l(-25/21)$, measured in the range $3.86° \leq \Theta \leq 27.49°$, completeness $\Theta max = 93.2\%$, 9 680 independent reflections, $R_{int} = 0.0733$, 5 232 reflections with $F_o > 4\sigma(F_o)$, 670 parameters, 0 restraints, $R1_{obs} = 0.1087$, $wR^2_{obs} = 0.2280$, $R1_{all} = 0.2027$, $wR^2_{all} = 0.2904$, GOOF = 1.077, largest difference peak and hole: 0.655 and −0.622 e Å^{-3}.

Experimental: The principle of the MCBJ technique is shown in Figure 2. A thin metal film (e.g., gold) with a lateral constriction was fabricated on top of a flexible, isolating substrate (phosphorous bronze covered with polyimide) by means of the electron-beam-lithography and lift-off technique (Figure 2A). Reactive ion etching was used to create a freestanding bridge. This MCBJ sample was mounted in a three-point bending mechanism (Figure 2B), and a bending force was applied to the bottom of the sample by a pushing rod (Figure 2C). This introduces surface extension, elongating the metal bridge, which finally breaks at its smallest constriction, creating two separated electrodes. The distance between the electrodes can be controlled in both the opening and closing direction with subpicometer accuracy by bending or relaxing the sample. Owing to the high surface mobility of gold, atomically sharp tips can be formed. Electrical characterization was performed using a Hewlett–Packard 4156B Parameter Analyzer. Further experimental details of our setup can be found elsewhere.[18] After the formation of two atomically sharp electrode tips, indicated by the observation of conductance quantization at room temperature, the distance between the leads was set to be longer than the length of the particular molecules under investigation. The molecules were then deposited out of much-diluted solution onto an open junction, and could thereby adsorb to one of the two electrodes. Subsequently, the system was evacuated. Once UHV conditions were reached, the junction with molecules applied was closed stepwise, and the current–voltage (I–V) characteristics were simultaneously measured. The closing procedure was reversed when the resistance was smaller than 12.9 kΩ, indicating a closed metal–metal bridge. Our system was fully automated, allowing the electrical-transport characteristics to be acquired simultaneously during repeated closing and opening cycles of the junction. Thereby, we observe a distinct region in which the molecular transport characteristics are measured.

Computational: DFT calculations were performed with the program package TURBOMOLE[27] using the BP86 functional.[28] For C, N, S, and H the TZVPP-basis (and auxiliary basis) set were employed, whereas for Ru the def-TZVP basis set with def-ecp pseudo potential was used.[29] First, the structure of the molecule with only two gold atoms was relaxed, then gold electrodes were added with the def-SV(P) basis set and def-ecp pseudo potential. Model geometries are shown in Figure SI 2a, Supporting Information, and the orbital flow analysis[30] is given in Figure SI 2b, Supporting Information. The transport calculations were performed with a home-made transport package based on the standard non-equilibrium Green's function technique.[31] Modeling of the self energies was done via absorbing boundary conditions with a leakage rate $\eta = 2.7$ eV. Absorption took place on the two layers of the model electrodes, see Figure SI 2b, Supporting Information, that are furthest away from the molecule. It was ascertained that the conclusions presented here are insensitive to the particular choice of these parameters.

Acknowledgements

This work was partially supported by the project "Inducing Charge States in Molecular Junctions" within the DFG priority program PP1243 and by the DFG Center for Functional Nanostructures at Karlsruhe University, Project B2.10. H. W.

and M. R. would like to thank the Deutsche Forschungsgemeinschaft (DFG) for financing within the priority program "Quantrans". We express our gratitude to O. Rubner and F. Weigand for their support with the TURBOMOLE program package and the DFT calculations. Also, we thank V. Meded for sharing his unpublished results. We are grateful to K. Fink and W. Riess for useful discussions and to C. Rettner for e-beam lithography.

[1] a) C. Joachim, J. K. Gimzewski, A. Aviram, *Nature* **2000**, *408*, 541; b) A. Nitzan, N. A. Ratner, *Science* **2003**, *300*, 1384.
[2] D. Djukic, K. S. Thygesen, C. Untiedt, R. H. M. Smit, K. W. Jacobson, J. M. van Ruitenbeek, *Phys. Rev. B* **2005**, *71*, 161402.
[3] a) L. H. Yu, D. Natelson, *Nano Lett.* **2004**, *4*, 79; b) H. S. J. van der Zant, Y.-V. Kervennic, M. Poot, K. O'Neill, Z. de Groot, J. M. Thijssen, H. B. Heersche, N. Stuhr-Jansen, T. Björnholm, D. Vanmaekelbergh, C. A. van Walree, L. W. Jenneskens, *Faraday Discuss.* **2006**, *131*, 347.
[4] a) X. H. Qui, G. V. Nazin, W. Ho, *Science* **2003**, *299*, 542; b) T. Morita, S. Lindsay, *J. Am. Chem. Soc.* **2007**, *129*, 7262.
[5] a) M. Ruben J.-M. Lehn, P. Müller, *Chem. Soc. Rev.* **2006**, *35*, 1056; b) N. Lin, S. Stepanow, F. Vidal, K. Kern, M. S. Alam, S. Stromsdorfer, V. Dremow, P. Müller, M. Ruben, *Dalton Trans.* **2006**, 2794; c) M. Ruben, *Angew. Chem. Int. Ed.* **2005**, *44*, 1594; d) M. S. Alam, S. Stromsdorfer, V. Dremow, P. Müller, M. Ruben, J.-M. Lehn, *Angew. Chem. Int. Ed.* **2005**, *44*, 7896.
[6] a) M. Mayor, C. von Hänisch, H. B. Weber, J. Reichert, D. Beckmann, *Angew. Chem. Int. Ed.* **2002**, *41*, 1183; b) S. A. Getty, C. Engtrakul, L. Wang, R. Liu, S.-H. Ke, H. U. Baranger, W. Yang, M. S. Fuhrer, L. R. Sita, *Phys. Rev. B* **2005**, *71*, 24140.
[7] J. Park, A. N. Pasupathy, J. I. Goldsmith, C. Chang, Y. Yalsh, J. R. Petta, M. Rinkoski, J. P. Sethna, H. D. Abruna, P. L. McEuen, D. C. Ralph, *Nature* **2002**, *417*, 722.
[8] a) T. Albrecht, A. Guckian, J. Ulstrup, J. G. Vos, *Nano Lett.* **2005**, *5*, 1451; b) T. Albrecht, K. Moth-Poulsen, J. P. Christensen, A. Guckian, T. Bjornholm, J. G. Vos, J. Ulstrup, *Faraday Discuss.* **2006**, *131*, 265.
[9] V. Balzani, A. Juris, M. Venturi, S. Campagna, S. Serroni, *Chem. Rev.* **1996**, *96*, 759.
[10] J.-P. Sauvage, J.-P. Collin, J.-C. Chambron, S. Guillerez, C. Coudret, V. Balzani, F. Barigelletii, L. de Cola, L. Flamigni, *Chem. Rev.* **1994**, *94*, 993.
[11] S. Rau, B. Schäfer, D. Gleich, E. Anders, M. Rudolph, M. Friedrich, H. Görls, W. Henry, J. G. Vos, *Angew. Chem. Int. Ed.* **2006**, *45*, 6215.
[12] a) M. K. Nazeeruddin, S. M. Zakeeruddin, J. J. Lagref, P. Liska, P. Comte, C. Barolo, G. Viscardi, K. Schenk, M. Grätzel, *Coord. Chem. Rev.* **2004**, *248*, 1317; b) Md. K. Nazeeruddin, C. Klein, P. Liska, M. Grätzel, *Coord. Chem. Rev.* **2005**, *249*, 1460; c) F. T. Kong, S. Y. Dai, K. J. Wang, *Chin. J. Chem.* **2007**, *25*, 168.
[13] a) J. D. Badjic, C. M. Ronconi, J. F. Stoddart, V. Balzani, S. Silvi, A. Credi, *J. Am. Chem. Soc.* **2006**, *128*, 1489; b) A. Petitjean, F. Puntoriero, S. Campagna, A. Juris, J. M. Lehn, *Eur. J. Inorg. Chem.* **2006**, 3878; c) V. Balzani, G. Bergamini, F. Marchioni, P. Ceroni, *Coord. Chem. Rev.* **2006**, *250*, 1254; d) S. Nitahara, N. Terasaki, T. Akiyama, S. Yamada, *Thin Solid Films* **2006**, *499*, 354.
[14] V. Balzani, A. Credi, S. Silvi, M. Venturi, *Chem. Soc. Rev.* **2006**, *35*, 1135.
[15] a) C. J. Muller, J. M. van Ruitenbeek, L. J. de Jongh, *Phys. C* **1992**, *191*, 485; b) J. Moreland, J. W. Elkin, *J. Appl. Phys.* **1985**, *58*, 3888.
[16] H. B. Weber, J. Reichert, F. Weigend, F. Ochs, D. Beckmann, M. Mayor, R. Ahlrichs, H. von Löhneysen, *Chem. Phys.* **2002**, *281*, 113.
[17] J. Reichert, R. Ochs, D. Beckmann, H. B. Weber, M. Mayor, H. von Löhneysen, *Phys. Rev. Lett.* **2002**, *88*, 1768904.
[18] E. Lörtscher, H. B. Weber, H. Riel, *Phys. Rev. Lett.* **2007**, *98*, 176807.
[19] a) V. Meded, A. Arnold, M. Ruben, F. Evers, unpublished; b) F. Evers, F. Weigend, M. Koentopp, *Phys. Rev. B* **2004**, *69*, 235411; c) F. Evers, K. Burke, *CRC Handbook on Molecular Electronics* (Ed: S. Lyshevsky), Taylor and Francis, London **2007**, Ch. 24; d) P. Schmitteckert, F. Evers, *Phys. Rev. Lett.* **2008**, *100*, 086401.
[20] M. Gerloch, E. C. Constable, *Transition Metal Chemistry*, Wiley-VCH, Weinheim **1994**.
[21] N. M. O'Boyle, T. Albrecht, D. H. Murgida, L. Cassidy, J. Ulstrup, J. G. Vos, *Inorg. Chem.* **2007**, *46*, 117.
[22] COLLECT, Data Collection Software; Nonius B.V., The Netherlands **1998**.
[23] Z. Otwinowski, W. Minor, in *Methods in Enzymology*, Vol. *276*, Part A (Eds: C. W. Carter, R. M. Sweet), Academic Press, New York **1997**, pp. 307–326.
[24] G. M. Sheldrick, *Acta Crystallogr. Sect. A* **1990**, *46*, 467.
[25] G. M. Sheldrick, SHELXL-97 (Release 97-2), University of Göttingen, Germany **1997**.
[26] CCDC-677855 (**1**) contains the supplementary crystallographic data for this paper. These data can be obtained free of charge via www.ccdc.cam.ac.uk/conts/retrieving.html (or from the Cambridge Crystallographic Data Centre, 12, Union Road, Cambridge CB2 1EZ, UK; fax: (+44) 1223-336-033; or deposit@ccdc.cam.ac.uk).
[27] K. Eichkorn, O. Treutler, H. Oehm, M. Haeser, R. Ahlrichs, *Chem. Phys. Lett.* **1996**, *242*, 652.
[28] a) A. D. Becke, *Phys. Rev. A* **1988**, *38*, 3098; b) J. P. Perdew, *Phys. Rev. B* **1986**, *33*, 8822.
[29] a) A. Schäfer, H. Horn, R. Ahlrichs, *J. Chem. Phys.* **1992**, *97*, 2571; b) K. Eichkorn, F. Weigend, O. Treutler, R. Ahlrichs, *Theor. Chem. Acc.* **1997**, *97*, 119; c) A. Schaefer, C. Huber, R. Ahlrichs, *J. Chem. Phys.* **1994**, *100*, 5829.
[30] F. Evers, A. Arnold, Molecular Conductance from Ab Initio Calculations: Self Energies and Absorbing Boundary Conditions, **2006**, http://arxiv.org/abs/cond-mat/0611401.
[31] A. Arnold, F. Weigend, F. Evers, *J. Chem. Phys.* **2007**, *126*, 17401.

Received: March 17, 2008
Revised: June 24, 2008

